BNL-207965-2018-TECH

EP&S/170

Using Monte Carlo methods to estimate occupational dosage during 225Ac production

D. Niedzielski, K. Yip

August 2018

Collider Accelerator Department

Brookhaven National Laboratory

U.S. Department of Energy

USDOE Office of Science (SC), Nuclear Physics (NP) (SC-26)

DISCLAIMER

Using Monte Carlo methods to estimate occupational dosage during ^{225}Ac production

Drake Niedzielski, Physics Department,
Rensselaer Polytechnic Institute, Troy, NY 12180

Kin Yip, Collider-Accelerator Department,
Brookhaven National Laboratory, Upton, NY 11973

August 10, 2018

Abstract

Since alpha emitting isotopes such as ^{225}Ac, ideal for radiation treatment, are in short supply, the Medical Isotope Research and Production program at Brookhaven National Laboratory (BNL) is developing new pathways for ^{225}Ac production. One proposed pathway is to resurrect the EBCO cyclotron at BNL to irradiate a ^{226}Ra target for 40 hours in a 16 MeV proton beam. Using MCNPX and CINDER software to simulate this process, we found that 1.26 Ci of ^{225}Ac could be produced from 300 mg of ^{226}Ra. To ensure workplace safety, we modeled the detailed geometry of lab 2-66C in Bldg. 801 and performed Monte Carlo simulations to estimate the radiation outside the lab as the irradiated sample is processed in a hot cell. We found the maximum dose outside the lab to be about 9×10^{-5} rem/h. To reduce occupational dose, we recommend $2''$ thick steel shielding covering the sample insertion passage. These ^{225}Ac production runs could help cover the EBCO cyclotron's operational costs.

1 Introduction

Alpha sources like ^{225}Ac are ideal for targeted radiation therapy. Possessing a high linear energy transfer, they can damage the DNA of nearby cancer cells while their short range mitigates damage to surrounding tissue.[1] ^{225}Ac is especially suited for radiation therapy due to its 10 day half-life, short enough to pass through the patient while allowing enough time for processing and distribution.[2] According to the DOE Isotope Program's customer feedback, the estimated demand for ^{225}Ac is roughly 50-100 Ci/year, however domestic supply is only about 1.5-1.7 Ci/year.[3] Additionally, the most popular method of production 'milks' ^{225}Ac from a ^{229}Th 'cow',[4] meaning that the supply of ^{225}Ac is limited by that of ^{229}Th. This is, obviously, not an ideal situation.

The Medical Isotope Research and Production (MIRP) program at Brookhaven National Laboratory (BNL) seeks to improve this situation and is currently developing new pathways for ^{225}Ac production. One

proposed pathway of interest is the low-energy cyclotron route, a (p, 2n) reaction shown in equation 1.

$$^{226}Ra + p \rightarrow \ ^{225}Ac + 2n \tag{1}$$

Previous studies indicate that this reaction has a cross section peak around 16 MeV.[5] The decommissioned EBCO TR-19 cyclotron at BNL would be resurrected for production runs, irradiating a ^{226}Ra target in a 16 MeV proton beam, exciting the reaction in equation 1. After 40 hours of total exposure over a period of 4 days, the irradiated sample would be transported to lab 2-66C in Bldg. 801 for further processing. It is this proposed project for which the authors hope to estimate the production yield and radiation hazard.

Using the Monte Carlo N-Particle eXtended (MCNPX) 2.7.0 and CINDER 1.05 software packages, we calculate the activity of each of the isotopes produced, including of course ^{225}Ac, and use those to compute the dosages at key locations inside and outside of lab 2-66C. We primarily focus on the dosages outside of the lab as they pose a less obvious hazard than those inside the lab. Performing the same dosage computations with additional shielding, we hope to bring the dosages outside the lab to consistently safe levels.

2 Methods

2.1 ^{225}Ac Production

300 mg of ^{226}Ra is deposited on an Al substrate. This sample is then put in either a 10° or 20° target head, which is then inserted into a target chamber. The target chamber is then placed in the EBCO cyclotron which will be operated at 16 MeV. The cyclotron's proton beam has a 1 cm diameter and a current of 200 μA. The beam will be run for 10 hours each day, allowing a 14 hour resting period, for a total of 4 days. The sample, now containing many new isotopes, is then taken to lab 2-66C in Bldg. 801 for further processing, where it will sit in a lead-shielded hot-cell.

2.2 Target, Hot-cell, and Simulation Setup

As shown in figure 1, the target apparatus that holds the ^{226}Ra sample consists of two separable parts: a target chamber and a choice of either a 10° or a 20° target head. An Al substrate, on which the ^{226}Ra is deposited, is inserted into a slot in the target head, at its respective angle. It is held down by a fastener plate with a rectangular hole in the middle to allow direct beam exposure. The target head is then inserted into the target chamber, posessing a bore hole for the proton beam to reach the ^{226}Ra sample. Both the 10° and 20° target apparatus were modeled as MCNPX input files based on scale-accurate schematics for the 20° target head sitting inside the target chamber. The 20° target head was modeled exactly according

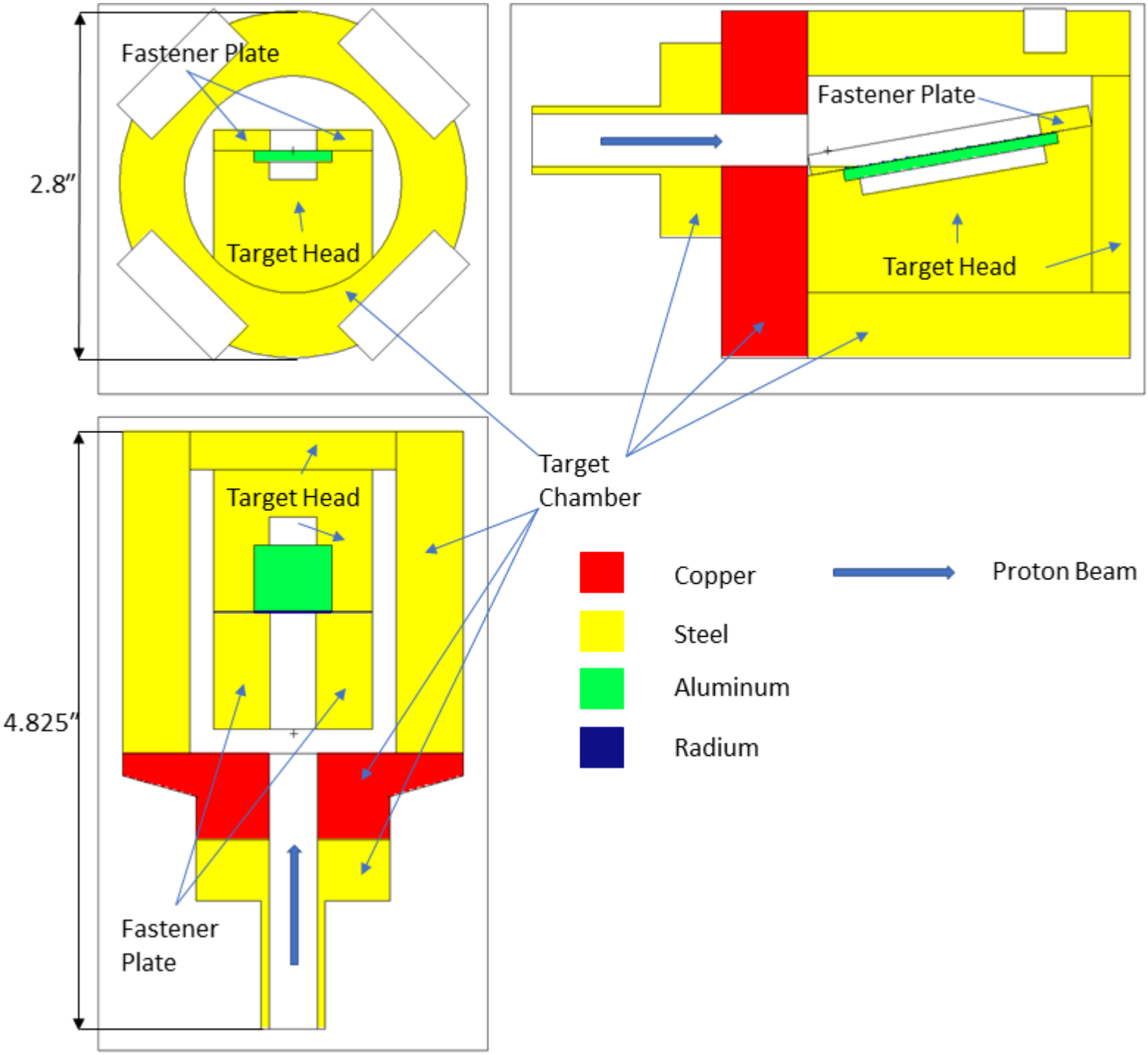

Figure 1: The 10° target apparatus is depicted above. MCNPX's geometry plotter was used to generate the 3 slices of the model in the XY, YZ and ZX planes. The white spaces represent vacuum in the model. The ^{226}Ra is very thinly deposited on the upper surface of the aluminum substrate and is barely visible even in color print.

to the schematics, but it was found that the angle was closer to 18° in the schematics. Since there were no specific schematics for the 10° target head, an exact 10° angle was used and the rest of the dimensions were chosen so that the effective area of the ^{226}Ra as seen by the proton beam matched the listed value in the schematics. The validity of the geometry was checked using the MCNPX geometry plotter.

For both targets, a 16 MeV proton source with a 1 cm diameter was used for regular simulation runs, but runs using 14 MeV and 19 MeV were done on the 10° target to explore the effects of beam energy on ^{225}Ac yield. MCNPX computations of neutron fluxes through the radium were performed on the input files using 1 node (32 cores) on the CORI supercomputer in NERSC.[1] A maximum of 35 million events were used to run the 10° target simulations and 50 million to run the 20° target simulations.[2]

The MCNPX output and history files were then used by CINDER to compute the abundances and activities of the isotopes produced from the radium. The production process history, 10 hours of beam exposure then 14 hours of decay, repeated for 4 days, was specified in CINDER's activation history and the 200μA of the beam was accounted for with the flux normalization factor, *snorm*, obtained by dividing by the charge of a proton, see equation 2. One of the input files that we used for CINDER activation, which contains the activation history and flux normalization, can be found in Appendix A.

$$snorm = \frac{200\mu A}{1.602 \times 10^{-19} C} = 1.248 \times 10^{15} s^{-1} \tag{2}$$

Finally, a gamma source script was run on the MCNPX and CINDER outputs to create gamma source cards (SDEF) of the irradiated target that are directly used as sources in MCNPX input files modeling lab 2-66C. In short, SDEF cards exist for 10° at 14, 16, and 19 MeV and for 20° at 16 MeV.

The detailed geometry of lab 2-66C in Bldg. 801, shown in figures 2 and 3, was modeled according to several blueprints and measurements made during a visit by the authors. The irradiated target was placed in the middle of the hot-cell adjacent to the fume-hood and aligned to the center of the insertion passage. Both hot cells have 6″ thick lead walls with thin steel coating, neglected in our model, and a lead-glass window for viewing. The source positioning represents a worst case scenario where there are paths for the radiation to escape the lab without passing through lead or concrete. Moving the sample away from the axis of the insertion passage would likely improve the outside dosages. At the time of writing, lab 2-66C does not have any door, thus it is absent in the model. Some of the blueprints used to construct the model were in contradiction with each other, reporting lengths of hot-cells that would not fit in the room. Measurement confirmed the author's suspicion that the reported hot-cell dimensions were a factor of two off. Additionally,

[1] The National Energy Research Scientific Computing Center (NERSC) in Berkeley, CA has several high performance computing systems of which CORI is one, http://www.nersc.gov/systems/cori .

[2] Number of events was chosen to keep simulation runs under a 4 hour time limit. The 20° target ran faster for some non-obvious reason.

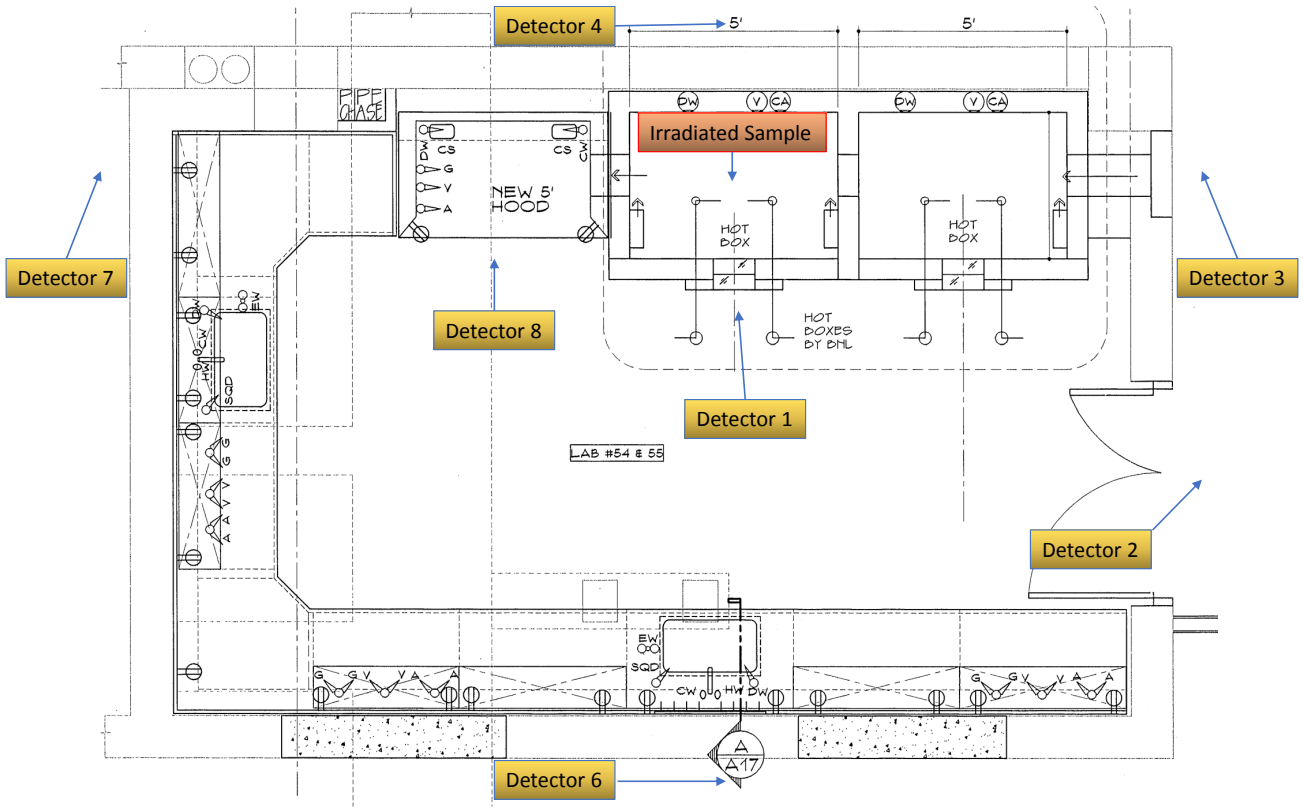

Figure 2: Shows the top view of lab 2-66C. Each of the detectors are placed 10 cm in front of the closest surface to help the tally error decrease faster. All detectors shown lie in the same plane as the irradiated sample. Detectors 1, 3, 4, 6, 7 are orthogonally in line with the sample, sharing either the same x or z coordinate. Detector 5, not shown, lies directly above the sample and is shown in figure 3.

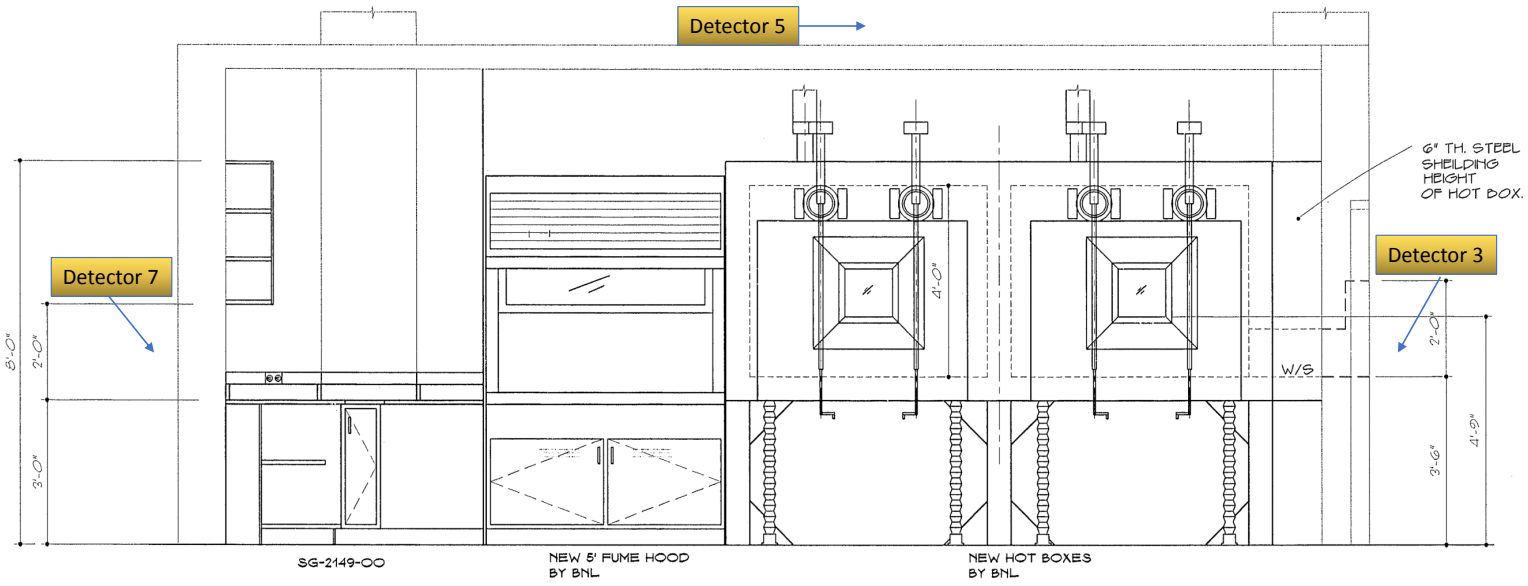

Figure 3: Shows the side view of lab 2-66C. Each of the detectors are placed 10 cm in front of the closest surface to help the tally error decrease faster. All detectors shown lie in the same plane as the irradiated sample.

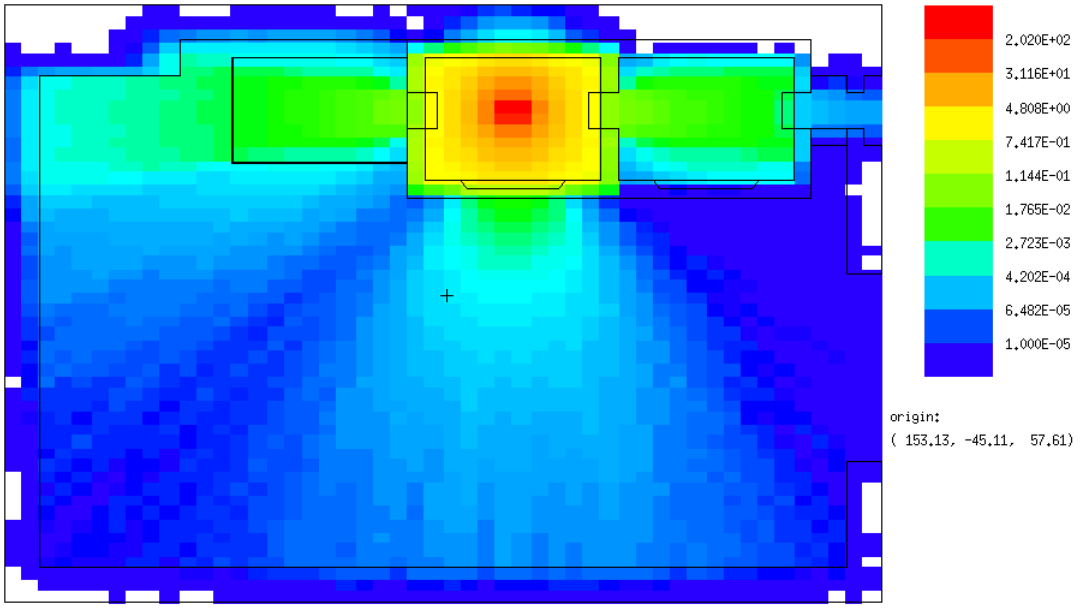

Figure 4: Shows the dosages across lab 2-66C from a top down view comparable to figure 2. A 10 degree target irradiated in a 16 MeV beam was used as the radiation source. The upper and lower cabinets are not visible in the model at the height level of the irradiated sample.

a thin piece of steel covering the wall recess and insertion passage is ignored in our original model and left as a variable shielding parameter.

MCNPX was used to estimate radiation dosages due to the irradiated sample at the locations shown in figures 2 and 3 with varying source type and shielding parameters. Estimations were done for the 10° and 20° sources in the absence of any additional shielding. For academic curiostiy, a simulation run using the 10° source was done without the self-shielding effects of the radium. In an effort to reduce dosage, runs were done using the 10° source with a steel shield covering the sample insertion passage, thickness varying from 0.5″ to 2″ in increments of 0.5″ . A mesh tally, shown in figure 4, was performed using the regular 10° source to produce a dosage map of lab 2-66C at the height level of the source. Finally, runs were done using the 10° source created with 14 and 19 MeV to explore the effect of beam energy on ^{225}Ac production.

3 Results and Discussion

Since the Al substrate that holds the radium is also subjected to the same beam exposure, we attempted to calculate its gamma spectrum using CINDER. However, the activity of the Al cell was 0 within the limitation of MCNPX. Thus, it suffices only to consider the effects of the radium when computing dosages in the model of lab 2-66C.

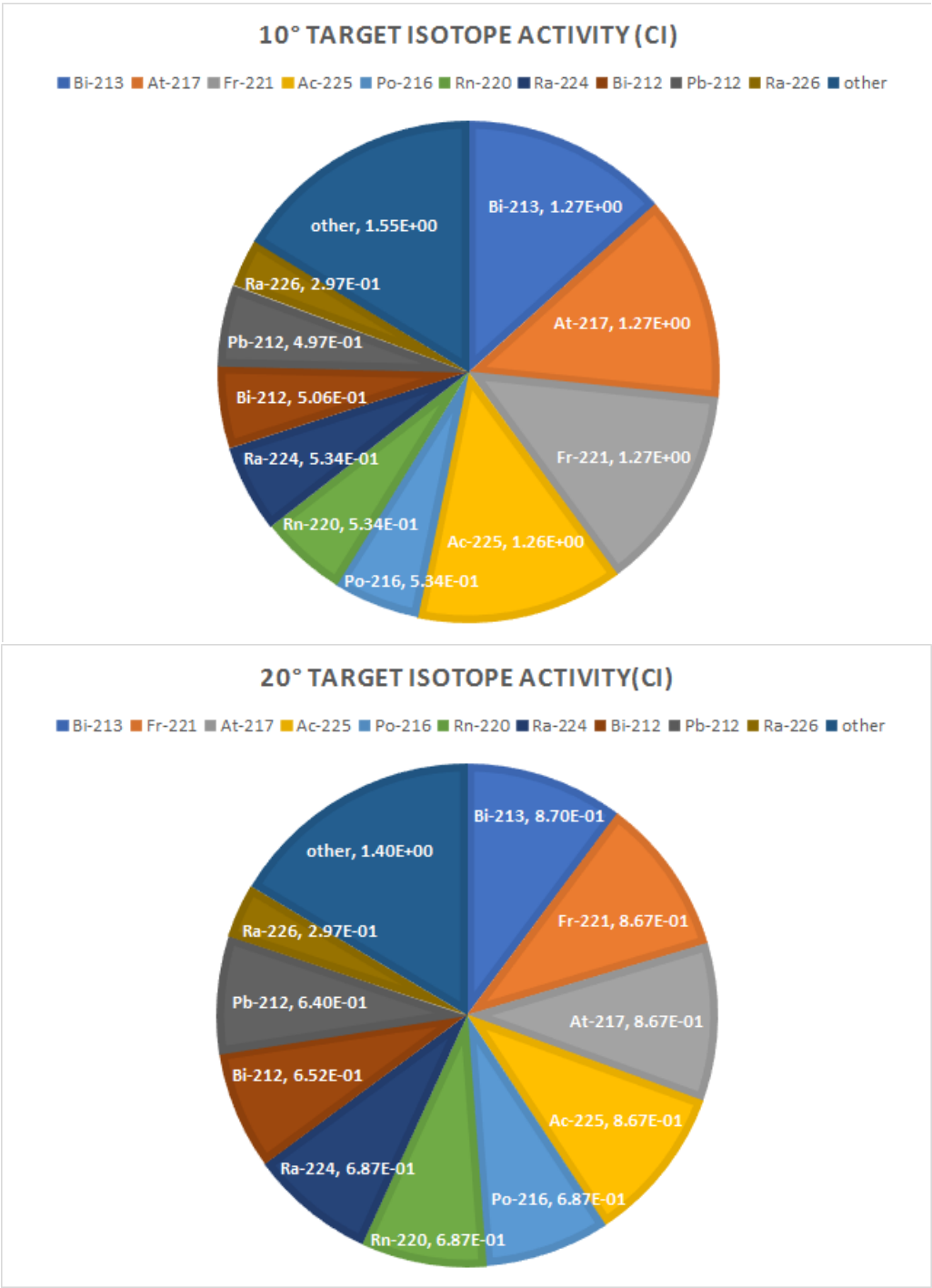

Figure 5: Shows the activity of each of the isotopes produced in the 10° and 20° irradiated samples using a 16 MeV proton beam. Total activities are 9.51 Ci and 8.52 Ci respectively.

Table 1: Dosages at detectors in figures 2 and 3, where the naked run had no ^{226}Ra layer but only the gamma source

Detector #	10° target [rem/h]	20° target [rem/h]	Naked 10° target [rem/h]
1	$2.00\times10^{-3}\pm1.0\%$	$2.50\times10^{-3}\pm0.9\%$	$2.09\times10^{-3}\pm0.5\%$
2	$4.33\times10^{-6}\pm0.9\%$	$5.43\times10^{-6}\pm0.8\%$	$4.43\times10^{-6}\pm0.8\%$
3	$8.81\times10^{-5}\pm0.8\%$	$1.13\times10^{-4}\pm0.8\%$	$1.10\times10^{-4}\pm0.6\%$
4	$1.10\times10^{-5}\pm9.9\%$	$1.61\times10^{-5}\pm9.4\%$	$1.04\times10^{-5}\pm6.2\%$
5	$3.10\times10^{-5}\pm4.1\%$	$4.03\times10^{-5}\pm4.4\%$	$3.52\times10^{-5}\pm5.9\%$
6	$2.38\times10^{-6}\pm16.4\%$	$3.01\times10^{-6}\pm14.2\%$	$2.45\times10^{-6}\pm19.7\%$
7	$2.11\times10^{-5}\pm5.7\%$	$2.99\times10^{-5}\pm6.7\%$	$2.48\times10^{-5}\pm5.6\%$
8	$5.79\times10^{-4}\pm0.5\%$	$6.95\times10^{-4}\pm0.5\%$	$6.00\times10^{-4}\pm0.5\%$

Table 2: Effect of Steel Shield Thickness on Detector 3 Dosages

Thickness [inches]	Dosage [rem/h]
0.0	$8.81\times10^{-5}\pm0.8\%$
0.5	$7.03\times10^{-5}\pm3.8\%$
1.0	$5.74\times10^{-5}\pm5.6\%$
1.5	$4.56\times10^{-5}\pm8.5\%$
2.0	$3.41\times10^{-5}\pm8.9\%$

After 40 hours of 16 MeV beam exposure, the 10° target had a total activity of 9.51 Ci while the 20° target had an activity of 8.52 Ci.[3] Of the total activities, ^{225}Ac accounted for 1.26 Ci and 0.87 Ci respectively, see figure 5. Thus the the 10° target is preferable from the standpoint of efficiency. Despite having a lower activity, the dosages around lab 2-66C are consistently higher with the 20° target see table 1. This is not contradictory, however, since the dose is due only to gamma radiation and dosage does not necessarily correlate linearly with activity, but depend on the energy distribution of the gamma radiation. So, from the standpoint of safety, the 10° target is also the preferable choice. Since the 10° target is the most preferable, unless otherwise specified, all other computations were done using the 10°/16 MeV sample as a source.

The location in the lab with the highest radiation dosage, excluding the inside of the hot-cell, is unsurprisingly just outside of the hot-cell looking into the lead-glass. With nothing else changed, the dosage is roughly 2×10^{-3} rem/h (detector 1). More importantly the highest dosage outside of the model lab 2-66C is right in front of the sample insertion passage. With no additional shielding the dosage is about 9×10^{-5} rem/h (detector 3).

With the addition of a $2''$ steel door covering the sample insertion passage the dosage can be brought down to about 3.5×10^{-5} rem/h, which is comparable to the dosage elsewhere outside the lab. See table 2 for more details. Despite the fact that lab 2-66C has no door at the time of writing, the dosage by the doorway is about 4.3×10^{-6} rem/h, which is low enough not to warrant additional shielding. In fact, the absence of a door could prove beneficial for the airflow to the fumehood in the lab.

[3]The accuracy of these figures are discussed in the final paragraph of this section.

Table 3: Dosages at detectors in figures 2 and 3 for 10° targets

Detector #	14 MeV target [rem/h]	16 MeV target [rem/h]	19 MeV target [rem/h]
1	$3.43\times10^{-4}\pm1.8\%$	$2.00\times10^{-3}\pm1.0\%$	$9.38\times10^{-3}\pm0.7\%$
2	$7.59\times10^{-7}\pm1.1\%$	$4.33\times10^{-6}\pm0.9\%$	$2.00\times10^{-5}\pm0.6\%$
3	$1.15\times10^{-5}\pm1.5\%$	$8.81\times10^{-5}\pm0.8\%$	$4.40\times10^{-4}\pm0.6\%$
4	$1.23\times10^{-6}\pm26.8\%$	$1.10\times10^{-5}\pm9.9\%$	$5.91\times10^{-5}\pm8.3\%$
5	$4.37\times10^{-6}\pm12.0\%$	$3.10\times10^{-5}\pm4.1\%$	$1.68\times10^{-4}\pm3.5\%$
6	$3.35\times10^{-7}\pm55.5\%$	$2.38\times10^{-6}\pm16.4\%$	$1.11\times10^{-5}\pm10.5\%$
7	$2.67\times10^{-6}\pm15.6\%$	$2.11\times10^{-5}\pm5.9\%$	$1.11\times10^{-4}\pm5.0\%$
8	$1.49\times10^{-4}\pm0.7\%$	$5.79\times10^{-4}\pm0.5\%$	$2.47\times10^{-3}\pm0.4\%$

For academic curiosity, we examined the self-shielding effects of the radium by removing the material cell from the simulation while leaving a naked source. We found that almost all locations had consistently higher dosages without self-shielding accounted for, but only slightly. At the location of interest, outside the insertion passage, the dosage without self-shielding was roughly 1.1×10^{-4} rem/h as opposed to 8.8×10^{-5} rem/h with self-shielding. See table 1 for more details. The non-self-shielding effect is small likely because the Ra-226 is very thin, 77.3 μm.

Studies conducted indicate that there should be a cross section peak for the ^{225}Ac producing reaction, equation 1, arround 16 MeV.[5] In our MCNPX simulations, we only used neutron interaction data for ^{226}Ra while proton interaction was computed with a model. Thus we were curious if MCNPX was able to reproduce results consistent with reference [5]. Performing the MCNPX simulation runs with 14 and 19 MeV proton beams, we found that they had total activities of 5.23 Ci and 20.57 Ci,[4] and respective ^{225}Ac yields of 0.99 Ci and 0.61 Ci. Both yields being less than the 1.26 Ci produced using the 16 MeV proton beam indicates a cross section peak somewhere between 14 and 19 MeV, consistent with reference [5]. A breakdown of the produced isotope activities can be found in Appendix B. Performing MCNPX dosage tallies at the detector locations, shown in figures 2 and 3, and using the irradiated targets created using 14 and 19 MeV beams, we found that higher energy beams produced consistently higher dosages. Those dosages are shown in table 3.

To check the reasonability of CINDER's isotope decay calculations, an activation run was done using the 10°/16 MeV MCNPX output and an extra 24 hours of decay after the 40 hour beam exposure over 4 days. Based on the Bateman equation for isotope activity decay, one expects the activity of the parent isotope to decay exponentially and the daughter isotope activities to approach that of the parent times the probability the parent decays into that daughter. We observed this behavior in the alpha decays of the 2 most prominent decay chains, ^{225}Ac and ^{224}Ra. However, the activities of the isotopes produced by beta decay in these 2 chains were occasionally very off from expected. The authors do not have a good explanation for this at the time of writing. Though this issue does not affect the activity of ^{225}Ac that we have found, it does put some

[4] Again, the accuracy of these figures is discussed in the final paragraph of this section.

doubt on the total activities from all isotopes stated in this report. This issue, however, does not affect the radiation dosages outside the hot-cell room as the dosage is due to the gamma radiation only.

4 Conclusion

Among all configurations that we attempted, the 10° target irradiated at 16 MeV gives the best ^{225}Ac yield. At 16 MeV, the 10° target head yields 1.26 Ci per 300 mg ^{226}Ra while the 20° head yields only 0.87 Ci per 300 mg ^{226}Ra. Additionally, the 10° target provides less of a radiation hazard inside and outside lab 2-66C as the irradiated sample is processed. Our estimated yields of ^{225}Ac using different beam energies are consistent with predictions of a previous study that a cross section peak for the reaction shown in equation 1 occurs around 16 MeV.[5]

The aluminum substrate on which the ^{226}Ra is deposited does not seem to contribute to the activity of the sample, validating our practice of examining only the irradiated sample activity. Due to the thinness of the ^{226}Ra layer, the self-shielding effect on the dosages is indeed very small.

The most significant source of error likely comes from the inability to take measurements of details inside the hot-cells and behind the sample insertion passage, e.g. the shape and thickness of the steel doors in the hot-cells. Exact dimensions were not given in the prints for lab 2-66C and had to be inferred from the scale of the drawings. Since these details are so close to the radiation source they may have some effect on the dosages at detectors in the same solid angle as viewed from the source.

5 Acknowledgements

I would like to thank my mentor, Kin Yip, for providing guidance, sharing his knowledge, and telling many stories throughout this summer. This project was supported in part by the U.S. Department of Energy, Office of Science, Office of Workforce Development for Teachers and Scientists (WDTS) under the Science Undergraduate Laboratory Internships Program (SULI).

Appendix A

```
title_lines
 DECAY_10deg_14MeV

files
 bigza_file /project/projectdirs/m1840_ec/cinder-1.05/data/bigza
 mcnpx_outp Ra_Target9.o
 mcnpx_histp histpe

run_options
 dname DECAY_10deg_14MeV-
 dcounter 1
 splprods 1
 tabular 1
 verbose 1

cinder_options
 tst 1.0e-5
 signif 1.0e-16
 kchn 0
 klib 0
 nfe 3
 nosame 0
 russ 1
 library /project/projectdirs/m1840_ec/cinder-1.05/data/c90lib0742

normalization
  snorm     1.248e+15

#run 10 hours, rest 14 hours
history
 1 1
  10.0 h
 1 0.0
  14.0  h
 1 1
  10.0 h
 1 0.0
  14.0  h
 1 1
  10.0 h
 1 0.0
  14.0  h
 1 1
  10.0 h
 1 0.0
  14.0  h

cell_list
 radium
 1
```

Appendix B

10°, 14 MeV		10°, 16 MeV		10°, 19 MeV		20°, 16 MeV	
Isotope	Activity [Ci]	Isotope	Activity [Ci]	Isotope	Activity [Ci]	Isotope	Activity [Ci]
Bi-213	9.95E-01	Bi-213	1.27E+00	Po-216	2.92E+00	Bi-213	8.70E-01
At-217	9.92E-01	At-217	1.27E+00	Rn-220	2.92E+00	Fr-221	8.67E-01
Fr-221	9.92E-01	Fr-221	1.27E+00	Ra-224	2.91E+00	At-217	8.67E-01
Ac-225	9.92E-01	Ac-225	1.26E+00	Bi-212	2.77E+00	Ac-225	8.67E-01
Ra-226	2.97E-01	Po-216	5.34E-01	Pb-212	2.72E+00	Po-216	6.87E-01
Po-218	1.53E-01	Rn-220	5.34E-01	Tl-208	9.94E-01	Rn-220	6.87E-01
Rn-222	1.53E-01	Ra-224	5.34E-01	Po-212	6.62E-01	Ra-224	6.87E-01
Pb-214	1.52E-01	Bi-212	5.06E-01	Bi-213	6.07E-01	Bi-212	6.52E-01
Bi-214	1.52E-01	Pb-212	4.97E-01	Fr-221	6.06E-01	Pb-212	6.40E-01
Ac-226	5.35E-02	Ra-226	2.97E-01	Ac-225	6.06E-01	Ra-226	2.97E-01
Rn-218	4.51E-02	Tl-208	1.82E-01	At-217	6.05E-01	Tl-208	2.34E-01
Ra-222	4.51E-02	Po-218	1.53E-01	Ac-224	4.83E-01	Po-218	1.53E-01
Th-226	4.51E-02	Rn-222	1.53E-01	Ra-226	2.97E-01	Rn-222	1.53E-01
Pb-209	3.76E-02	Pb-214	1.52E-01	Po-218	1.53E-01	Pb-214	1.52E-01
Tl-209	2.09E-02	Bi-214	1.52E-01	Rn-222	1.53E-01	Bi-214	1.52E-01
Xe-135	5.24E-03	Po-212	1.21E-01	Pb-214	1.52E-01	Ac-224	1.14E-01
I-133	4.78E-03	Ac-224	8.84E-02	Bi-214	1.52E-01	Ac-226	6.04E-02
In-115*	4.30E-03	Ac-226	7.58E-02	Ac-226	1.06E-01	Rn-218	5.09E-02
Cd-115	4.06E-03	Rn-218	6.39E-02	Rn-218	8.97E-02	Ra-222	5.09E-02
Ag-109*	4.00E-03	Ra-222	6.39E-02	Ra-222	8.97E-02	Th-226	5.09E-02
Pd-109	3.99E-03	Th-226	6.39E-02	Th-226	8.96E-02	Pb-209	3.29E-02
Ce-143	3.95E-03	Pb-209	4.79E-02	At-216	4.84E-02	Tl-209	1.83E-02
I-132	3.58E-03	Tl-209	2.66E-02	Fr-220	4.84E-02	At-216	1.14E-02
Te-132	3.41E-03	At-216	8.86E-03	Ra-225	2.70E-02	Fr-220	1.14E-02
Sn-121	3.31E-03	Fr-220	8.86E-03	Pb-209	2.29E-02	Ag-112	6.46E-03
Ag-112	3.17E-03	In-115*	8.05E-03	Xe-135	1.83E-02	I-133	5.94E-03
Rh-105	3.13E-03	I-133	7.98E-03	Ce-143	1.80E-02	Ra-225	5.92E-03
Y-93	2.78E-03	Cd-115	7.51E-03	I-133	1.46E-02	Ag-109*	5.73E-03
Pd-112	2.75E-03	Rh-105	6.83E-03	Tl-209	1.28E-02	Pd-109	5.73E-03
Pm-149	2.35E-03	Xe-135	6.48E-03	Ag-112	1.10E-02	Pd-112	5.47E-03
Xe-133	2.34E-03	Ag-112	6.14E-03	I-132	1.09E-02	Rh-105	5.16E-03
Sr-91	2.18E-03	Ag-109*	5.56E-03	As-77	1.04E-02	Ce-143	4.79E-03
Ag-113	2.13E-03	Pd-109	5.56E-03	Te-132	1.04E-02	In-115*	4.71E-03
Mo-99	2.08E-03	I-132	5.37E-03	Pd-112	9.38E-03	I-132	4.46E-03
Tc-99*	1.91E-03	Ce-143	5.18E-03	Sr-91	9.35E-03	Cd-115	4.36E-03
I-135	1.74E-03	Pd-112	5.17E-03	Y-93	8.03E-03	Te-132	4.21E-03
As-77	1.49E-03	Te-132	5.06E-03	Pr-145	7.63E-03	As-77	3.93E-03
La-140	1.46E-03	Ra-225	4.84E-03	Xe-133	7.57E-03	Xe-135	3.92E-03
Nb-97	1.39E-03	As-77	4.24E-03	Ag-109*	7.20E-03	Sn-121	3.80E-03
Y-91*	1.38E-03	Sn-121	4.09E-03	Pd-109	7.20E-03	Pm-149	3.48E-03
Sb-127	1.36E-03	Xe-133	3.57E-03	Mo-99	6.99E-03	Kr-85*	3.00E-03
Y-92	1.34E-03	Y-93	3.53E-03	Tc-99*	6.68E-03	Y-92	2.90E-03
Ag-111	1.33E-03	Pm-149	3.44E-03	I-131	6.37E-03	Pm-151	2.82E-03
Kr-85*	1.33E-03	Kr-85*	3.42E-03	Sb-127	6.35E-03	Xe-133	2.76E-03
Zr-97	1.29E-03	Y-92	3.20E-03	Rh-105	6.33E-03	Sr-91	2.47E-03

Nb-97*	1.23E-03	Nb-97	3.19E-03	I-135	6.17E-03	Y-93	2.38E-03
La-141	1.16E-03	Ag-111	3.12E-03	In-115*	6.15E-03	La-140	2.31E-03
Te-127	1.13E-03	Zr-97	2.96E-03	Y-91*	5.93E-03	Nb-97	2.17E-03
Ba-140	1.01E-03	Nb-97*	2.81E-03	La-140	5.93E-03	Zr-97	2.01E-03
Te-129	9.35E-04	Mo-99	2.60E-03	Sn-121	5.84E-03	Ba-140	1.98E-03
I-131	7.97E-04	Ba-140	2.60E-03	Te-127	5.84E-03	I-131	1.96E-03
Sb-129	7.93E-04	La-140	2.54E-03	Y-92	5.74E-03	Nb-97*	1.91E-03
Ru-105	7.89E-04	Tc-99*	2.38E-03	Ba-140	5.68E-03	Ag-111	1.88E-03
Nd-147	7.13E-04	Sr-91	2.35E-03	Cd-115	5.64E-03	Pr-145	1.81E-03
Pr-143	6.27E-04	Pm-151	2.23E-03	La-141	5.29E-03	Mo-99	1.76E-03
Ra-225	6.19E-04	I-135	2.20E-03	Kr-85*	5.11E-03	Ag-113	1.75E-03
Pr-145	6.01E-04	Te-129	2.02E-03	Pm-149	4.89E-03	Kr-83*	1.70E-03
Br-82	5.77E-04	Ag-113	1.98E-03	Kr-83*	4.53E-03	Tc-99*	1.61E-03
Kr-83*	5.17E-04	Ru-105	1.89E-03	Nb-97	3.65E-03	Nd-147	1.60E-03
Ce-141	5.14E-04	Nd-147	1.88E-03	Ag-111	3.51E-03	Y-91*	1.57E-03
I-130	5.08E-04	I-131	1.86E-03	Zr-97	3.39E-03	Sm-153	1.52E-03
Y-90	4.91E-04	Sb-127	1.83E-03	Nb-97*	3.22E-03	Te-127	1.39E-03
Rb-88	4.91E-04	Sb-129	1.75E-03	Br-82	3.19E-03	Ru-105	1.35E-03
Kr-88	4.40E-04	Te-127	1.74E-03	Pr-143	3.15E-03	Te-129	1.33E-03
Y-87	4.13E-04	Kr-83*	1.72E-03	Pm-151	3.00E-03	La-141	1.32E-03
In-117*	4.03E-04	Pr-145	1.67E-03	Te-129	2.59E-03	Sb-127	1.18E-03
Pm-151	3.92E-04	La-141	1.60E-03	Nd-147	2.51E-03	I-135	1.16E-03
Sr-89	3.89E-04	Y-91*	1.49E-03	Ag-113	2.49E-03	Sb-129	1.12E-03
Po-216	3.78E-04	Sb-128	1.33E-03	Ce-141	2.49E-03	As-76	9.09E-04
Rn-220	3.78E-04	Sm-153	1.28E-03	Sb-129	2.21E-03	Pr-143	9.06E-04
Ra-224	3.78E-04	I-130	1.14E-03	Ge-77	2.12E-03	Ge-77	8.62E-04
Bi-212	3.59E-04	As-76	1.06E-03	Y-90	1.93E-03	Y-90	7.32E-04
Pb-212	3.53E-04	Br-82	1.02E-03	Rb-88	1.72E-03	I-130	7.24E-04
In-117	3.32E-04	Ge-77	1.01E-03	Ru-105	1.68E-03	In-117	7.12E-04
Ru-103	3.22E-04	Pr-143	9.06E-04	Kr-88	1.54E-03	Sm-156	6.38E-04
Rh-103*	3.22E-04	Rb-88	7.95E-04	I-130	1.49E-03	Rb-88	6.32E-04
Ba-135*	3.02E-04	Ce-141	7.51E-04	Te-131*	1.47E-03	Zr-89	6.07E-04
Nb-96	3.02E-04	Sm-156	7.44E-04	Sb-128	1.43E-03	Y-89*	6.06E-04
Pr-142	2.94E-04	Kr-88	7.12E-04	Br-83	1.39E-03	Nb-96	6.04E-04
Ga-72	2.90E-04	Nb-95*	7.12E-04	Ga-72	1.38E-03	In-117*	5.99E-04
Sb-119	2.90E-04	Zr-89	7.08E-04	Sr-89	1.36E-03	Ce-141	5.88E-04
Zn-72	2.88E-04	Y-89*	7.07E-04	Sb-122	1.19E-03	Br-82	5.83E-04
Xe-135*	2.84E-04	Nb-96	7.05E-04	Zn-72	1.10E-03	Ga-72	5.66E-04
Sm-153	2.76E-04	In-117	6.87E-04	Cs-136	1.05E-03	Kr-88	5.66E-04
I-123	2.62E-04	Ga-72	6.45E-04	Xe-135*	1.01E-03	Zn-72	5.61E-04
Y-87*	2.59E-04	Zn-72	6.40E-04	Y-91	9.67E-04	Y-86	5.47E-04
Sb-128	2.41E-04	Y-86	6.39E-04	In-117*	9.47E-04	Br-83	5.23E-04
Sb-122	2.39E-04	Sr-89	6.33E-04	Ga-73	9.31E-04	Te-131*	5.21E-04
Cs-136	2.25E-04	In-117*	5.81E-04	Ge-73*	9.19E-04	Sr-89	4.86E-04
Y-91	2.25E-04	Y-90	5.61E-04	Sm-153	8.41E-04	Sb-122	4.77E-04
Rh-105*	2.25E-04	Rh-105*	5.39E-04	Sr-92	8.19E-04	Sr-92	4.35E-04
Zr-89	2.16E-04	Br-83	5.26E-04	In-117	7.95E-04	Nb-95*	4.07E-04

Y-89*	2.15E-04	Sr-92	4.89E-04	Br-77	7.60E-04	Cs-132	4.07E-04
Nb-95*	2.04E-04	Pd-111*	4.35E-04	Ru-103	7.03E-04	Ru-103	4.00E-04
Ga-73	2.01E-04	Ag-111*	4.26E-04	Rh-103*	7.02E-04	Rh-103*	3.99E-04
Ge-73*	1.98E-04	Ru-103	4.18E-04	Y-87	6.38E-04	Xe-133*	3.96E-04
Sr-92	1.87E-04	Rh-103*	4.17E-04	Rb-82*	6.13E-04	Rh-105*	3.84E-04
Ge-77	1.58E-04	Xe-135*	3.59E-04	As-76	6.06E-04	Ga-73	3.10E-04
Br-83	1.58E-04	Ba-135*	3.53E-04	Xe-133*	5.94E-04	Ge-73*	3.06E-04
Cd-117	1.33E-04	Sr-83	3.48E-04	Pr-142	5.92E-04	Y-91	3.03E-04
Tl-208	1.29E-04	Pr-142	3.43E-04	Br-76	5.65E-04	Sr-83	2.99E-04
Pd-111*	1.24E-04	Pd-111	3.42E-04	Y-86	5.61E-04	La-135	2.95E-04
Ag-111*	1.22E-04	Eu-157	3.26E-04	Eu-157	5.34E-04	Rh-100	2.94E-04
Rn-217	1.19E-04	Sb-122	2.78E-04	Cs-131	4.89E-04	Pr-142	2.94E-04
Rb-86	1.10E-04	Y-91	2.69E-04	Cu-67	4.88E-04	Eu-157	2.79E-04
Xe-133*	1.08E-04	Cd-117*	2.36E-04	Rh-105*	4.77E-04	Sb-128	2.70E-04
Sn-125	1.06E-04	I-124	2.16E-04	Zr-95	4.66E-04	Cd-117*	2.47E-04
Te-131*	1.05E-04	Eu-156	2.14E-04	Sm-156	4.51E-04	Cd-117	1.91E-04
Cs-131	9.78E-05	Rh-101*	2.11E-04	Zr-89	4.21E-04	Xe-135*	1.90E-04
Pd-111	9.77E-05	Te-131*	1.96E-04	Y-89*	4.21E-04	Eu-156	1.84E-04
Po-212	8.61E-05	Cd-117	1.87E-04	Nb-95*	4.08E-04	Rh-101*	1.81E-04
Te-129*	8.30E-05	Pm-148	1.82E-04	As-78	3.95E-04	Rb-86	1.65E-04
Zr-95	8.11E-05	Xe-133*	1.81E-04	Rb-86	3.84E-04	Rb-84	1.61E-04
Ac-224	6.19E-05	Cs-136	1.75E-04	Xe-131*	3.37E-04	Zr-95	1.55E-04
Cd-115*	5.75E-05	Cs-132	1.58E-04	Te-131	3.30E-04	Te-129*	1.36E-04
As-74	5.73E-05	Rn-217	1.52E-04	Cd-117	3.12E-04	Pd-111*	1.24E-04
As-78	5.06E-05	Rb-84	1.51E-04	Nb-96	3.02E-04	Ag-111*	1.22E-04
Cd-117*	4.88E-05	Rb-86	1.28E-04	Tc-95	2.97E-04	Te-131	1.17E-04
Y-90*	4.10E-05	Xe-129*	1.23E-04	La-135	2.95E-04	As-74	1.15E-04
Te-125*	3.74E-05	Ga-73	1.21E-04	Kr-79	2.95E-04	As-78	1.11E-04
I-125	3.61E-05	Ge-73*	1.20E-04	Rh-100	2.94E-04	Xe-129*	1.05E-04
Tl-210	3.18E-05	Zr-95	1.14E-04	Sb-119	2.90E-04	Rn-217	1.04E-04
Nd-149	3.06E-05	Cs-131	1.14E-04	Nb-90	2.73E-04	Rb-81	1.02E-04
At-218	3.06E-05	Te-129*	1.14E-04	Cs-132	2.71E-04	Cs-131	9.78E-05
Ce-144	2.98E-05	Br-80	1.09E-04	Ru-97	2.30E-04	Pd-111	9.77E-05
Pr-144	2.98E-05	Br-80*	1.01E-04	Ce-144	2.12E-04	Br-80	9.31E-05
Xe-127	2.93E-05	As-78	9.87E-05	Pr-144	2.12E-04	Br-80*	8.69E-05
Sr-85	2.93E-05	Ce-144	8.65E-05	Ce-137	2.09E-04	Ce-144	8.54E-05
La-142	2.80E-05	Pr-144	8.65E-05	Te-129*	2.07E-04	Pr-144	8.54E-05
Ba-136*	2.52E-05	Xe-127	6.83E-05	Sn-125	1.98E-04	Xe-131*	8.48E-05
Te-127*	2.41E-05	As-74	6.69E-05	Eu-156	1.96E-04	Ru-106	6.83E-05
Te-131	2.36E-05	Ru-106	6.16E-05	Sb-126	1.92E-04	Rh-106	6.83E-05
Ru-106	2.23E-05	Rh-106	6.16E-05	Rb-81	1.85E-04	Sn-125	6.64E-05
Rh-106	2.23E-05	Sn-125	4.71E-05	Tc-96	1.80E-04	Nb-95	5.71E-05
Tc-95*	1.78E-05	La-142	4.48E-05	As-74	1.72E-04	Nd-149	4.21E-05
Nb-91*	1.75E-05	Te-131	4.41E-05	Rb-84	1.61E-04	Y-90*	4.10E-05
Nb-95	1.35E-05	Nd-149	4.09E-05	Pm-148	1.56E-04	La-142	3.78E-05
Sb-124	1.35E-05	Nb-95	3.98E-05	Nb-95	1.32E-04	Po-212	3.61E-05
Rb-83	1.27E-05	Cs-134*	3.65E-05	Cd-117*	1.26E-04	Tl-210	3.18E-05

A * next to an isotope indicates a meta-stable nuclear isomer.

References

[1] S. Kojima, J. Cuttler, N. Shimura, H. Koga, A. Murata, and A. Kawashima, "Present and future prospects of radiation therapy using α-emitting nuclides," *Dose Response*, vol. 16, p. 1–8, 2018.

[2] B. Allen, "Systemic targeted alpha radiotherapy for cancer," *J. Biomed. Phys. Eng.*, vol. 3, p. 67–80, 2013.

[3] C. Cutler, "Ebco cyclotron for ac-225 production startup and operating cost," Dec. 2017. Project proposal by the Medical Isotope Research and Production Program.

[4] D. Scheinberg and M. M. Devit, "Actinium-225 in targeted alpha-particle therapeutic applications," *Curr Radiopharm*, vol. 4, pp. 306–320, 2011.

[5] C. Apostolidis, R. Molinet, J. McGinley, K. Abbas, J. Mollenbeck, and A. Morgenstern, "Cyclotron production of ac-225 for targeted alpha therapy," *Applied Radiation and Isotopes*, vol. 62, pp. 383–387, 2005.